Implementation and analysis of list mode algorithm using tubes of response on a dedicated brain and breast PET

L. Moliner[a], C. Correcher[b], A.J. González[a,*], P. Conde[a], L. Hernández[a], A. Orero[a], M.J. Rodríguez-Alvarez[a], F. Sánchez[a], A. Soriano[a], L.F. Vidal[a], J.M. Benlloch[a]

[a] *Instituto de Instrumentación para Imagen Molecular (I3M). Centro Mixto UPV CSIC CIEMAT. Camino de Vera s/n, 46022, Valencia, Spain.*
[b] *ONCOVISION (GEM-Imaging S.A.) 46012, Valencia, Spain.*

Abstract

In this work we present an innovative algorithm for the reconstruction of PET images based on the List-Mode (LM) technique which improves their spatial resolution compared to results obtained with current MLEM algorithms. This study appears as a part of a large project with the aim of improving diagnosis in early Alzheimer disease stages by means of a newly developed hybrid PET-MR insert. At the present, Alzheimer is the most relevant neurodegenerative disease and the best way to apply an effective treatment is its early diagnosis. The PET device will consist of several monolithic LYSO crystals coupled to SiPM detectors. Monolithic crystals can reduce scanner costs with the advantage to enable implementation of very small virtual pixels in their geometry. This is especially useful for LM reconstruction algorithms, since they do not need a pre-calculated system matrix. We have developed an LM algorithm which has been initially tested with a large aperture (186 mm) breast PET system. Such an algorithm instead of using the common lines of response, incorporates a novel calculation of tubes of

*Instituto de Instrumentación para Imagen Molecular (I3M)
Email address: agonzalez@i3m.upv.es (A.J. González)

response. The new approach improves the volumetric spatial resolution about a factor 2 at the border of the field of view when compared with traditionally used MLEM algorithm. Moreover, it has also shown to decrease the image noise, thus increasing the image quality.

Keywords: PET, Monolithic scintillators, Image reconstruction, LM Reconstruction

---

1. Introduction

The use of monolithic crystals has shown a great potential since it allows for a virtual pixelation during the reconstruction process. However, when maximum likelihood expectation maximization (MLEM)[(1)] or ordered subset expectation maximization (OSEM)[(2)] reconstruction algorithms are considered, such a pixellation can not be entirely exploited due to the need of a storage system matrix that restricts the minimum size of virtual pixels. LM algorithms[(3)] do not require a pre-calculated system matrix. They compute the intersection image elements for each line of response (LOR) or tube of response (TOR) and their associated weights on the fly.

All the aforementioned algorithms, MLEM, OSEM or LM, use backprojectors. The ideal backprojector collects all image elements that are crossed by lines of sight between a given pair of detectors and evaluates the area (or volumes) of intersection between the fan of lines and the collected squares or cubes (voxels). One of the most popular backprojector is the tracing of a ray through an array of pixels or voxels using the Siddon method[(4)]. This method models LORs, but thin lines do not match well the area of the detector pixels. Thus, a pair of detectors could be more accurately modeled if a TOR linked the detectors. This technique has been established in last years with successful results using both square[5] and cylindrical[6] sections of the TORs.

In this work, an LM algorithm was implemented for a dedicated breast PET that uses monolithic crystals, with the aim to study the effect of different virtual pixel sizes on the reconstructed images. In this implementation, the TOR method based on square sections was used as a new backprojector. Such an approach is an extension of the Siddon method[4] for volumes. Due to easy calculations taken around the Siddon intersection point, is possible to reach a high computational efficiency. To evaluate the performances of this algorithm, studies on the system spatial resolution, uniformity, and image quality were carried out and they were compared with those obtained with LM-Siddon and MLEM algorithms. The MLEM we have implemented in this work uses as backprojector the solid angle approach[7].

2. TOR method

In this section we present a description of the TOR backprojector. The image space is considered as intersection volumes of orthogonal sets of parallel planes. The data space is formed by the set of coincidences collected in the detector pixels. Therefore, TORs are defined by a coincidence volume connecting two of these detector pixels, so they are cuboids crossing the image space which is formed by voxels. In our calculation, all intersections will be approximated to squared areas. So, the area of intersection TOR-voxels will always be the same as the area of the chosen virtual pixel.

Considering a fixed pixel size we use the central point of the TOR to trace a line between the considered pixels. Then, we compute the intersection point be-

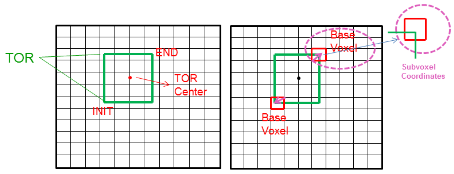

Figure 1: Intersection between TOR and a plane formed by the faces of the voxels in the image space (left). Voxel coordinates referred to its own axis (right).

tween this line and the nearest plane formed by the voxel faces. Knowing this intersection point as well as the area of the TOR and taking into account the squared area approximation mentioned above, we can obtain the *INIT* and *END* points on the image plane as shown in Fig. 1. These ones concern to the intersection points between the edges of the TOR and the image space, and have minimum and maximum voxel indexes respectively according to our voxel indexation. In order to find out the crossed areas by the TOR, we will refer the points *INIT* and *END* to its own reference system, see Fig. 1.

Finally, using these coordinates and knowing the voxel indexes involved in the intersection we can further compute all the voxel areas. In a volumetric approximation, the product of these area values for every voxel times the length of the TOR path for the central point between two consecutive planes will be performed.

3. Measurements and results

The LM-TOR algorithm has been initially evaluated on the dedicated breast PET MAMMI[(8)]. The MAMMI ring is formed by twelve detector modules. Every one consists of a pyramidal truncated LYSO monolithic crystal of 40×40 mm^2 entrance surface and 10 mm height coupled to a PSPMT[(9–11)].

The exploration is carried out in prone position avoiding breast compression and allowing for a more comfortable patient position. Data are acquired in 3D and are stored in list mode format. The acquisition system allows for coincidences among one module and its seven opposite, defining a total of 42 pairs. The MLEM reconstruction used voxels of 1 mm (at three space directions) and pixels of 2×2 mm^2, respectively[11,8].

3.1. Spatial resolution

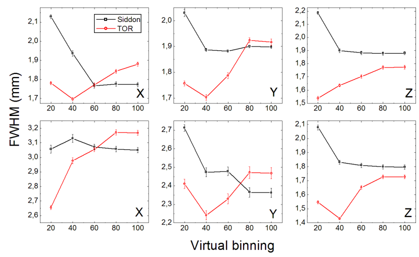

Figure 2: Spatial resolution (FWHM) versus the number of pixels for the transaxially centered source and for the three axis (top). The same for a 70 mm transaxially displaced point source (bottom).

The FWHM of a reconstructed ^{22}Na point-like source of a 1 mm in diameter and about 37 kBq, was used to study the spatial resolution performance of the system. The point source was placed in two different positions (center and 70 mm offset) of the transaxial field of view (FoV) and centered at the axial FoV. The acquisition time for each position was 5 minutes. Twelve iterations were applied for LM-TOR, LM-Siddon and MLEM reconstructions. For the LM approach, the virtual considered pixellation was 20×20, 40×40, 60×60, 80×80, 100×100 (corresponding to pixel sizes of 2×2 mm^2, 1×1 mm^2, 0.67×0.67 mm^2, 0.5×0.5 mm^2 and 0.4×0.4 mm^2, respectively). Two voxel size of 0.5 mm and 1 mm were taken into account. The reconstruction results for LM-TOR and LM-Siddon for 1 mm voxel size are shown in Fig. 2. Here, the FWHM for X, Y and Z projections are represented versus the number of pixels. We observe that Siddon method tends to reduce the spatial resolution when the pixel size decreases. In contrast to these results, the TOR approach shows the best spatial resolution values for the largest pixel sizes. We expect a higher signal to noise ratio for larger pixel sizes since there are more LORs contained in such a pixel. Both, TOR and Siddon seem to converge into similar values when the pixel size decreases, due to the fact that the differences between the two approximations diminishes too.

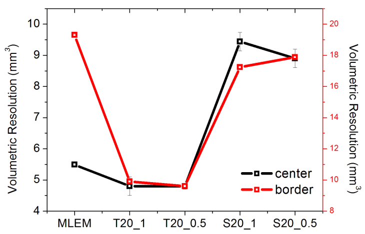

Figure 3: Volumetric spatial resolution using MLEM, LM-TOR and LM-Siddon. The index following the applied reconstruction method acronym on the X-axis, indicates the voxel cubic size.

In Fig. 3 we compare the volumetric resolutions of LM-TOR, LM-Siddon for voxel sizes of 1 mm and 0.5 mm with MLEM (using 1 mm voxel size). In all cases the virtual detector pixel size was set to 20×20. Due to storage limitations the voxel sizes for MLEM reconstructions could not be further reduced. With MLEM we observe a considerable difference between the results provided by the two source positions, while using LM-TOR or LM-Siddon this difference is almost vanished. The best values for the spatial resolution are achieved when LM-TOR reconstruction is underused. This is about 50% better than Siddon and MLEM at the FoV border. The differences when using voxels of 1 mm and 0.5 mm are not significative.

3.2. *Uniformity*

To evaluate the uniformity a cylindrical phantom was specially designed and placed at the center of the transaxial FoV and covering the entire axial FoV. It was 40 mm height and 100 mm in diameter. The initial activity was 43 kBq/ml and the acquisition lasted 10 minutes. The attenuation correction was applied during the reconstruction process following an image segmentation approach[11]. The chosen voxel size for all reconstructions was 1 mm. The uniformity was computed as the ratio between *(Voxel*$_{max}$*- Voxel*$_{min}$*)* over *(Voxel*$_{max}$*+ Voxel*$_{min}$*)*[12] in a volume of interest of 30 mm.

The results for LM-Siddon are most of times slightly higher than those observed for LM-TOR. When using binnings of 20×20 or 40×40, the uniformity values for LM-TOR and LM-Siddon reach values of about 20% and 24%, respectively. However for a pixellation of 60 $\times$ 60 or higher with LM-TOR method the values of the uniformity are comparable to MLEM (20 $\times$ 20), and reasonable good as presented elsewhere[11] with clinical images.

3.3. *Image quality*

Another custom cylindrical phantom (see Fig. 4) reproducing several hot and cold lesions has also been designed to evaluate the image quality. It was filled with a warm background activity concentration of 6 kBq/ml. Four cylindrical inserts placed 30 mm away from the center of the phantom were filled with different activity concentrations to model the hot and cold lesions. The cold one was 26 mm in diameter and filled with a non radiactive solution. Two of the hot lesions had a size of 20 mm in diameter and were filled with an activity concentration about eight and four times higher than the background activity, respectively. The third one was 15 mm in diameter and was filled with and activity concentration eight times higher than the background activity. The analyzed data were reconstructed using 1 mm voxel size.

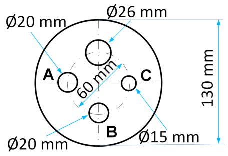

Figure 4: Phantom designed to evaluate the image quality. CC have been calculated in hot lesions A, B and C.

We determined the so-called contrast coefficients (CC) for the three hot lesions with the labels A, B and C in Fig. 4, calculating the activity ratio of a ROI over the background divided by the real measured activity ratio[13,14], as follows:

$$CC = \frac{measured\ insert\ activity/measured\ background}{real\ insert\ activity/real\ background} \tag{1}$$

The insert ROIs had dimensions of 80% their nominal size. The background ROIs were centered in the phantom with identical dimensions to the particular insert ROI. The CC results for the LM-TOR when using binnings of 80×80 become comparable to those obtained with MLEM. For the number of pixels ranging from 20×20 to 60×60, the values of LM-TOR are on average slightly lower than those determined with MLEM. However, the CC obtained with LM-Siddon are closer to MLEM when the largest pixels sizes (20×20) are considered.

4. Conclusions and future work

The MLEM algorithm using the solid angle approximation to precalculate the system matrix and the LM algorithm using both Siddon and TOR approaches,

Image Quality	CC (A)	CC (B)	CC (C)
MLEM (20×20)	0.77	0.90	0.86
LM-TOR (20×20)	0.54	0.73	0.7
LM-TOR (40×40)	0.56	0.75	0.69
LM-TOR (60×60)	0.59	0.72	0.7
LM-TOR (80×80)	0.74	0.87	0.86
LM-Siddon (20×20)	0.62	0.85	0.83
LM-Siddon (40×40)	0.59	0.79	0.74
LM-Siddon (60×60)	0.50	0.70	0.69
LM-Siddon (80×80)	0.58	0.73	0.7

Table 1: CC for different reconstruction binnings using MLEM, LM-TOR and LM-Siddon

have been compared. The spatial resolution analysis shows that the TOR method improves the image spatial resolution compared to the other methods, being this benefit higher at the edges of the FoV. The TOR method achieves acceptable values of uniformity at detector pixel sizes below 0.67×0.67 mm^2. The CC values for the TOR method improve when the binning increases, achieving the best results at 0.5×0.5 mm^2. This occurs since the smallest pixel sizes permit a more accurate localization of the line of response which results on a better CC determination.

The use of different detector pixel sizes allows for different image reconstruction features. With the TOR method, the virtual detector pixel size of 1×1 mm^2, shows the best average results in terms of spatial resolution, while larger pixel binning provides better uniformity and image quality.

An extensive work is undergoing to include the solid angle approach in LM for direct comparison. Moreover, an alternative reconstruction, the LM-OSEM is under implementation. This method is expected to deliver faster reconstruction times, enabling on-line reconstructions.

Acknowledgement

This work was supported by the Centre for Industrial Technological Development co-funded by FEDER through the Technology Fund (DREAM Project, IDI-20110718), by the Spanish Plan Nacional de Investigación Científica, Desarrollo e Innovación Tecnológica (I+D+I) under Grant. No. FIS2010-21216-CO2-01TEO 2008/114.

References

[1] L.A. Shepp, Y. Vardi, Maximum likelihood reconstruction for emission tomography, IEEE Trans. Medical Imaging MI-2 (1982) 113–122.

[2] H.M. Hudson, R.S. Larkin, Accelerated Image Reconstruction Using Ordered Subsets of projection Data, IEEE. Trans. Med. Img. 13 (1994) 601–609.

[3] A.J. Reader, R.Manavaki, S. Zhao, P.J. Julyan, D.L. Hastings, J. Zweit, Accelerated List-Mode EM Algortihm, IEEE Trans. Nucl. Sc. 49 (2002) 42–49.

[4] R.L. Siddon, Fast calculation of the eact radiological path for a three-dimensional CT array, Med. Phys. 12 (1985) 252–255.

[5] C. Schretter, A fast tube of response ray-tracer, Med. Phys. 33 (2006) 4744–4748.

[6] G. Pratx, S. Surti, C. Levin, Fast List-Mode Reconstruction for Time-of-Flight PET Using Graphics Hardware, IEEE Trans. Nucl. Sc. 58 (2011) 105–109.

[7] A.V. Oosteron, J. Strackee, The solid angle of a Plane Triangle, Trans. Bio. Eng. 12 (1983) 125-126.

[8] J.A. González, T.S. Aukema, J. Barberá, J.M. Benlloch, C. Correcher, A. Orero, A. Soriano, W. Vogel, C. Vázquez, L.F. Vidal, R.A. Valdés, Design and First Results of an Innovative and Dedicated Breast PET, Current Medical Imaging Reviews 8 (2012) 144–150.

[9] J.M. Benlloch, V. Carrilero, A.J. González, J. Catret, Ch.W. Lerche, D. Abellán, F. García de Quirós, M. Giménez, J. Modia, F. Sánchez, N. Pavón, A. Ros, J. Martínez, A. Sebastiá, Scanner calibration of a small animal PET camera based on continuous LSO crytals and flat panel PSPMTs, NIM-A 571 (2007) 26–29.

[10] F. Sánchez, J.M. Benlloch, B. Escat, N. Pavón, E. Porras, D. Kadi-Hanifi, JA. Ruiz, F.J. Mora, A. Sebastiá, Design and test of portable mini gamma camera, Med. Phys 31(6) (2004) 1384–1397.

[11] A. Soriano, A.J. González, A. Orero, L. Moliner, M. Carles, F. Sánchez, J.M. Benlloch, C. Correcher, V. Carrilero, M. Seimetz, Attenuation correction without transmission scan for the MAMMI breast PET, NIM-A 648 (2011) 75–78.

[12] Report of AAPM Nuclear Medice Comittee, Quantitation of SPECT Performance, Med. Phys. 22 (1995).

[13] NEMA Standadrs Publication NU 2-2007, Performance measurements of Positron Emission Tomographs. NEMA Standards.(2007)

[14] NEMA Standadrs Publication NU 4-2008, Performance measurements of Small Animall Positron Emission Tomographs. NEMA Standards.(2008)